Carbon dispersed iron-manganese catalyst for light olefin synthesis from CO hydrogenation

Jianli Zhang*,, Kegong Fang*, Kan Zhang*, Wenhuai Li*, and Yuhan Sun*,†**

*State Key Laboratory of Coal Conversion, Institute of Coal Chemistry, Chinese Academy of Sciences,
Taiyuan, Shanxi 030001, P. R. China
**Graduate University of the Chinese Academy of Sciences, Beijing 100039, China

Abstract−High performance iron-manganese catalysts dispersed with carbon to produce light olefins from CO hydrogenation were prepared by sol-gel method using citric acid as precursor. The effects of carbon content on the bulk structure, the water gas shift reaction, the chain propagation ability and the activity and selectivity of the catalysts were investigated. The results showed that the catalysts were gradually reduced during the decomposition of the precursor when calcined under pure N_2. The formation of iron-manganese mixed crystallites was favored and stabilized because of the enhanced interaction of iron and manganese with increasing carbon content. During the subsequent CO hydrogenation reaction, all the catalysts showed high activity and olefin selectivity. With increasing carbon content, the water gas shift (WGS) reaction was restrained and the chain propagation ability was inhibited. Catalysts with higher carbon content showed much lighter hydrocarbon products; however, the selectivity of CH_4 was almost unchanged.

Key words: CO Hydrogenation, Fe-Mn Catalyst, Light Olefin, Selectivity, Chain Propagation Ability

INTRODUCTION

Direct synthesis of light olefin from CO hydrogenation has been considered as a possible solution and practical interest to meet the great demands for chemical feedstocks such as ethylene, propylene and butylenes, which may provide a more economical way than the conventional methods such as catalytic cracking of naphtha and dehydrogenation of alkanes. In recent years, many efforts have been made on the direct synthesis of light olefins from CO hydrogenation, and catalysts with high olefin selectivity have been developed [1-10]. Particularly, iron-manganese catalysts have been extensively investigated [6-10] that exhibit high activity and olefin selectivity with low methane selectivity. However, at the present time, the yield and selectivity of light olefins are far from optimal, due to the limitation of Anderson-Schulz-Flory (A-S-F) distribution in Fischer-Tropsch synthesis and secondary reactions such as hydrogenation and polymerization of primary olefin products [11]. Therefore, catalysts with high selectivity and yields to produce light olefins as the desired products still need to be further investigated, and enhancing the olefin selectivity and controlling the product distribution are still the main problems. It is known that unsupported iron-manganese catalyst prepared by coprecipitation method usually gives a broad spectrum of products, especially much heavier hydrocarbons (C_5+), which often provides a low productivity of light olefins. Also, for supported catalysts, the nature of the supports such as the acidity usually decreased the olefin selectivity. To obtain high yields of light olefins, inhibition of the chain propagation ability and reduction of CH_4 selectivity are practical and realizable; hence, this paper mainly aims at the above two aspects over a carbon dispersed Fe-Mn cat-alyst prepared from sol-gel method. Particular attention was focused on the effects of carbon and its correlation with catalytic performance.

EXPERIMENTAL

1. Catalyst Preparation

A series of iron manganese catalysts with different carbon content were prepared by sol-gel method. The typical preparation of catalysts were as follows: First, the aqueous solutions of $Fe(NO_3)_3 \cdot 9H_2O$ and $Mn(NO_3)_2$ (50 wt% aqueous solution) with a desired Fe/Mn molar ratio of 3/1 were prepared separately and mixed together; then, a certain amount of citric acid was added to the solution under constant stirring (citric acid/metallic ions molar ratio=0.2), and afterwards, K_2CO_3 solution was dropped slowly into the solution (Fe/K molar ratio=60/1). Finally, a small amount of HNO_3 was added to adjust the pH value of the solution. The final solution was kept in a water bath at 333 K until the solution became a gel, and then the as-prepared gel was dried at 393 K for 24 h and calcined in a quartz tube under high pure N_2 at 673 K for 4 h. The calcined sample was cooled to room temperature and passivated by O_2/N_2 (2 v% O_2) for 4 hours. The other three samples with different citric acid and metallic ions ratios (0.4, 0.6 and 0.8, respectively) were prepared with the same procedures as related above.

A precipitated sample denoted as Scp without the presence of citric acid, used as comparison, was coprecipitated from a mixed aqueous solution of iron and manganese nitrate with a desired Fe/Mn molar ratio of 3/1 by using ammonia as precipitator. The obtained precipitates were washed with deionized water, filtered and dried at 353 K for 24 h, following calcining in air at 723 K for 1.5 h, and then the obtained sample was impregnated with potassium carbonate (2 wt%) by incipient wetness method, following dried at 353 K for 24 h. The sample was first reduced in situ at 553 K for 12 h at atmospheric pressure with gas flow rate of 1.05 $Nl/g_{cat} \cdot h$.

2. Catalyst Tests and Product Analysis

The catalytic properties of all the samples were performed in a pressurized fixed bed flow reactor in the following conditions: total pressure=1.5 MPa, H_2/CO=2 : 1 (molar feed ratio), gas flow rate=1.05 Nl/g$_{cat}$·h, T=603 K. In all cases, typically 2.0 ml of the catalysts was employed.

The feed gas and the products were all analyzed offline with gas chromatographs (GC). A thermal conductivity detector with carbon molecular sieve packed column (2 m×3 mm i.d., Ar carrier) was used to detect H_2, CO, CO_2 and CH_4 in the feed gas and tail gas. The light hydrocarbons (C_1-C_4) in the feed gas and the oxygenates in the water, collected in an ice trap equipped on the outlet of the reactor, were detected by using a flame ionization detector with a Porapak Q packed column (2 m×3 mm i.d., Ar carrier); the liquid hydrocarbons were analyzed by flame ionization detector with a OV-101quartz capillary column (60 m×0.25 mm i.d., N_2 carrier). And the C_1-C_4 hydrocarbons in the tail gas were analyzed by using a flame ionization detector equipped with an octadecane packed column (1.5 m×3 mm i.d., N_2 carrier).

The material balance was based on carbon and the results were presented in terms of activity by CO conversion (X_{CO}), light olefin selectivity by olefin to paraffin ratio (O/P) in the C_2-C_4 fraction; the hydrocarbon distribution was expressed as the weight percentage of desired components in all the hydrocarbons.

3. Catalyst Characterization

3-1. Carbon Content Analysis (CHN)

All the samples with different carbon content were analyzed on a Vario EL Analyzer. Each sample was tested three times, and the final value was the average.

3-2. BET Surface Area Measurement

The textural properties of the catalysts were determined from the isotherms of N_2 physisorption at 77 K with a Micromeritics Digisorb 2600 system. The samples were degassed at 383 K for 4 h in vacuum prior to the determination of the adsorption isotherm.

3-3. X-Ray Diffraction (XRD)

X-Ray diffraction (XRD) analysis was conducted on a Rigaku D/Max 2500 powder diffractometer using Cu Kα radiation as X-ray source at 40 kV and 40 mA. The 2θ angles were scanned from 20° to 90°.

3-4. Temperature Programmed Reduction (TPR)

H_2-TPR experiments were performed by using conventional TPR equipment monitored with a thermal conductivity detector (TCD). The reducing gas consisted of 5 vol% hydrogen in Ar at a flow rate of 20 cm^3/min. The TPR profiles were recorded by heating the samples from 323 K to 1,073 K at a linear heating rate of 10 K/min. In all the experiments, the weight of the sample used was 50 mg and the size was 40-60 mesh.

3-5. Scanning Electron Microscopy (SEM)

The particle morphology of the catalysts prepared by sol-gel method was observed by means of a Hitachi S-570 scanning electron microscopy. Also, the morphology of a coprecipitated (cp) sample with the same metal composition was used as comparison.

RESULTS AND DISCUSSION

1. Carbon Content Analysis

The carbon content of the samples after being calcined under N_2

Table 1. Carbon content of the catalysts

Samples	Citric acid/metallic ions molar ratio	Carbon content (wt%)
S_1	0.2	0.23
S_2	0.4	0.66
S_3	0.6	2.43
S_4	0.8	6.66

Table 2. The textural properties of the catalysts

Samples	Surface area (m^2/g)	Volume (cm^3/g)	Pore size (nm)
S_1	153.69	0.24	6.34
S_2	38.13	0.15	15.45
S_3	56.17	0.11	8.04
S_4	77.54	0.10	5.23

is listed in Table 1. It can be seen that the carbon content was increased with increasing precursor proportion when calcined in pure N_2 atmosphere; however, the increase of carbon content was not proportionate to the original composition of the samples.

2. BET Surface Area Measurement

The textural properties of the catalysts with different carbon content are shown in Table 2. At low carbon content, the sample shows high surface area, which is comparable with that of the catalyst prepared by controlled degradation method [12]. With increasing carbon content, the surface area is firstly decreased and then increased; contrary to this, the pore size shows a reverse change. The initial decrease of the surface area was mainly caused by the reduction of the sample during the decomposition of the precursors without enough oxidant, which could also be proved from Fig. 1 and Fig. 2. With the increase of carbon content, the catalysts are further reduced; how-
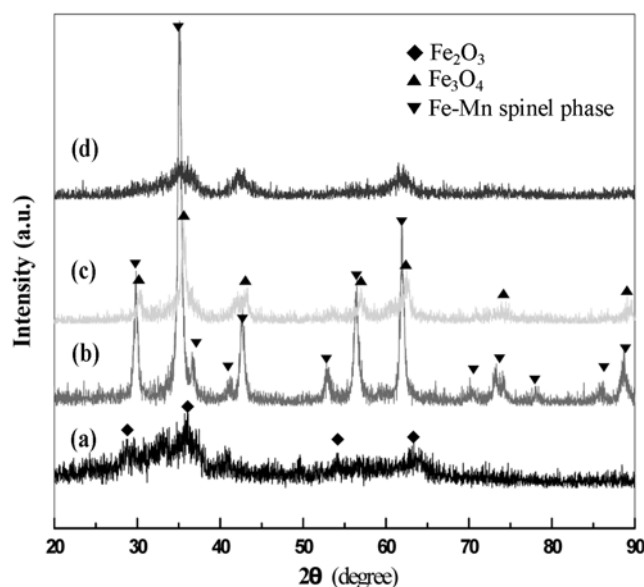
Fig. 1. The XRD patterns of the catalysts.
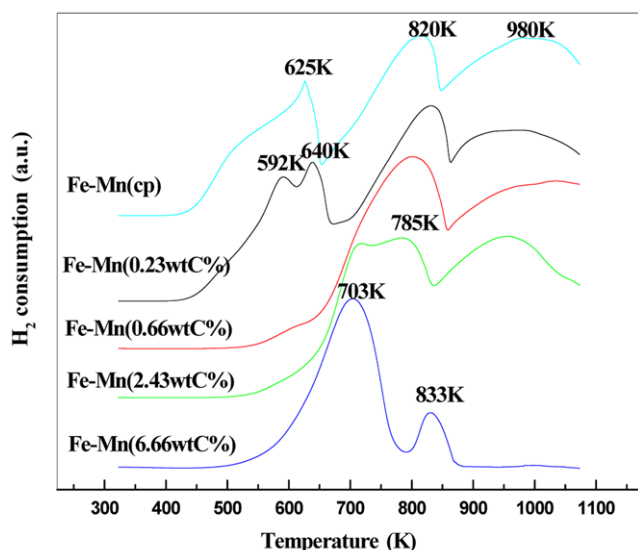(a) 0.23 wtC%; (b) 0.66 wtC%; (c) 2.43 wtC%; (d) 6.66 wtC%.

Fig. 2. The H₂-TPR profiles of the catalysts.

ever, the disperse effect of carbon becomes the pivotal factor for the increase of surface area.

3. X-Ray Diffraction Characterization

The bulk structures of the catalysts are shown in Fig. 1. At low carbon content, the sample shows low intensity peaks suggesting that the sample prepared by sol-gel method is well dispersed, and only Fe_2O_3 could be identified. With increasing carbon content, magnetite and iron-manganese spinel phase are approved in the bulk structure, indicating that the samples are gradually reduced. The formation of carbon facilitated the formation of iron-manganese mixed crystallites. At high carbon content, the catalysts were further dispersed and showed broad diffraction peaks. In all the samples, no graphite peak ($2\theta=27°$) was found in the XRD patterns suggesting that the carbon formed during the decomposition of the precursor was in an amorphous state. Also, no iron carbide was found in the XRD patterns, since the decomposition of the precursor was at low temperature (below 473 K), and only the reduction of the catalysts happened, or the carbon retarded the formation of single iron crystallites and hence the carburization of iron, which would be discussed below.

4. H₂-TPR Characterization

The H₂-TPR experiments were used to characterize the influence of carbon and its content on the reduction behavior of the catalysts. The profiles of the catalysts with different carbon content are shown in Fig. 2. The TPR profile of coprecipitated (cp) iron-manganese catalyst with the same metal composition was used as comparison. Evidently, the onset temperature of reduction shifted to higher temperature with increasing carbon content when compared with coprecipitated sample, suggesting that the catalysts had been partially reduced by the incomplete decomposition of precursor before the H₂-TPR experiment. A sharp peak at around 703 K that appeared with the carbon content above 2.43 wt% was attributed to the reduction of an $(Fe,Mn)_3O_4$ mixed spinel phase to manganowustite, and a small peak at the temperature range 823 K to 873 K was attributed to the reduction of cubic $FeMnO_3$ to manganowustite [13]. The high-temperature broad peak at around 980 K may be associated with the reduction of Fe^{3+} ions dissolved in MnO [13]; however, almost no reduction peak was found in this region in the sample with 6.66 wt% carbon, suggesting that this sample was stabilized mainly in two iron-manganese mixed crystallites, that is, $(Fe,Mn)_3O_4$ mixed spinel phase and cubic $FeMnO_3$, which were hard to reduce to metallic iron with high carbon content. So, it could be concluded that the formation of carbon not only promoted the interaction of iron and manganese, but also stabilized the iron-manganese mixed crystallites. It could also be suggested that a mixed structure of iron and manganese with strong interaction without single iron crystallite such as iron carbide and α-Fe could be prepared.

5. The SEM Analysis

The SEM micrographs of Fe-Mn catalysts are shown in Fig. 3. Most of the particles prepared by coprecipitated method (Fig. 3(a)) are irregularly shaped with sharp edges and the surface of the particles seems nearly smooth. However, the catalyst prepared by sol-gel process shows much more coarse surface (Fig. 3(b)), which may be caused by the dispersion of amorphous carbon, especially, when incorporated with K_2CO_3 (Fig. 3(c)); the particle size of most grains is slightly decreased and many small grains are attached to large grains. The carbon formed from the decomposition of precursors seemed to prevent the aggregation of the small particles, which gave a much different morphology from that of the coprecipitated sample, and may cause much different catalytic behaviors as could be seen from Table 3.
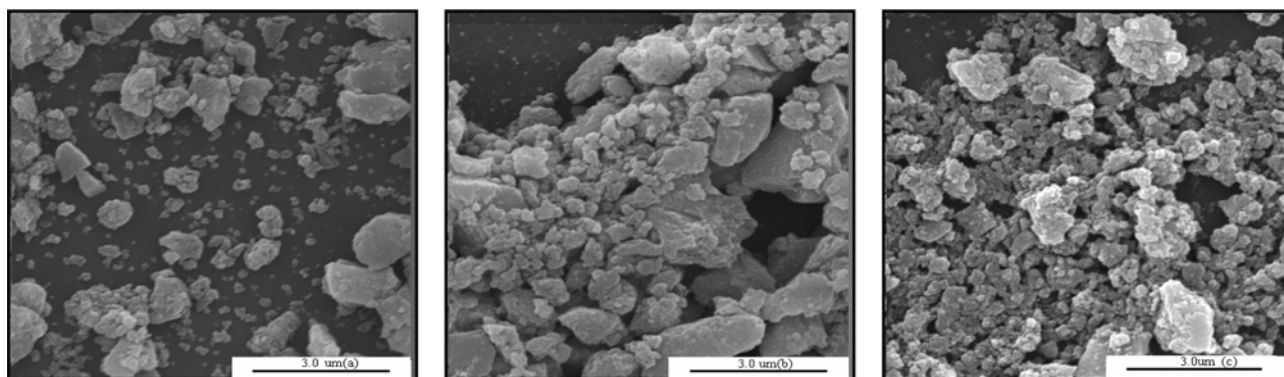

Fig. 3. The SEM images of the catalysts.
        (a) Fe-Mn (coprecipitated), (b) Fe-Mn (sol-gel), (c) Fe-Mn-K (sol-gel).

Table 3. Catalytic performance of the catalysts

Samples	CO conv. (%)	H$_2$ conv. (%)	CO$_2$ sel.	Product distribution (wt%)			O/P	Productivity (g/[m^{3}N(CO+H$_2$)])	
				CH$_4$	C$_2^=$~C$_4^=$/C$_2^0$~C$_4^0$	C$_5$+		C$_2^=$~C$_4^=$	C$_5$+
S$_1$	96.49	75.87	31.01	20.98	36.87/7.24	34.91	5.09	49.35	46.72
S$_2$	96.19	75.56	29.68	21.85	37.97/7.67	32.51	4.95	55.00	47.09
S$_3$	98.40	78.64	28.17	21.73	40.35/8.26	29.66	4.89	60.35	44.37
S$_4$	97.01	75.23	28.14	21.23	39.09/8.20	31.48	4.77	52.53	42.31
S$_{cp}$[a]	95.51	74.68	32.45	21.97	33.76/7.23	37.05	4.67	41.47	45.53

[a]Coprecipitated sample.

Reaction conditions: P=1.5 MPa, T=603 K, WHSV=1.05 Nl/g$_{cat}$·h, H$_2$/CO=2/1.

6. Catalytic Performances of the Catalysts

The catalytic performances of the catalysts are shown in Table 3. The properties of a coprecipitated sample are also listed. The coprecipitated sample shows lowered olefin selectivity and much C$_5$+ products in the hydrocarbon distribution. For the catalysts prepared by sol-gel process, all the samples showed high activity with CO conversion up to 96%. Although the olefin selectivity was slightly decreased with increasing carbon content, all the samples showed high olefin selectivity with maximum olefin to paraffin (O/P) ratio of 5.0, which was superior to the ultrafine iron manganese catalyst [8]. Especially, the CH$_4$ content was almost invariable and the C$_5$+ selectivity was decreased with the increase of carbon content, suggesting that the hydrogenation ability was not enhanced and the formation of heavy hydrocarbons was inhibited with increasing carbon content, that is, the formation of C$_2$-C$_4$ fraction was favored. In all the samples, the catalyst with 2.43 wt% carbon content showed the highest olefin productivity, and the total C$_2$-C$_4$ content was nearly 49 wt% in all the hydrocarbons, which was approximate to the maximum value of 56% by Anderson-Schulz-Flory distribution [14].

7. Effect of Carbon Content on the Chain Propagation Ability

Fig. 4 shows the effect of carbon content on the chain propagation ability and the corresponding overall C$_2$-C$_4$ fraction of the catalysts. Evidently, the chain propagation probability (α) was greatly reduced by the increase of carbon content. The α value was under

0.55 when the carbon content was above 2.43 wt%, which showed a maximum C$_2$-C$_4$ fraction of 49 wt%. Considering the byproduct of methane, an α value of 0.45 to 0.55 was favorable. However, an α value above 0.60 was often obtained on an unsupported Fe-Mn catalyst and the C$_2$-C$_4$ fraction would be below 50% [8]. In our experiment, with in situ incorporation of carbon into the catalyst, the chain propagation ability was remarkably inhibited. It can also be seen from Table 3 that with increasing carbon content, the C$_5$+ selectivity was obviously decreased. It is evident that the formation of carbon was helpful to inhibit the chain propagation. The effect of carbon may have the same role in inhibiting the chain propagation as carbonaceous deposit [15]. It was thought that the carbonaceous deposit could change the distribution of hydrocarbons to favor the formation of short chain hydrocarbons. The presence of carbon was retained on sites of formation of high hydrocarbons and blocked these sites. Also, with increasing carbon content, the formation of Fe-Mn mixed crystallite was promoted. It was thought that the Fe-Mn spinel crystallite favored the formation of light hydrocarbons [12], especially light olefin products, due to the strong interaction of iron and manganese. So, the formation of carbon partially blocked the active site to inhibit the formation of long chain hydrocarbons. At the same time, the existence of carbon made hardly reducible Fe-Mn mixed crystallite, which also favored the forma-
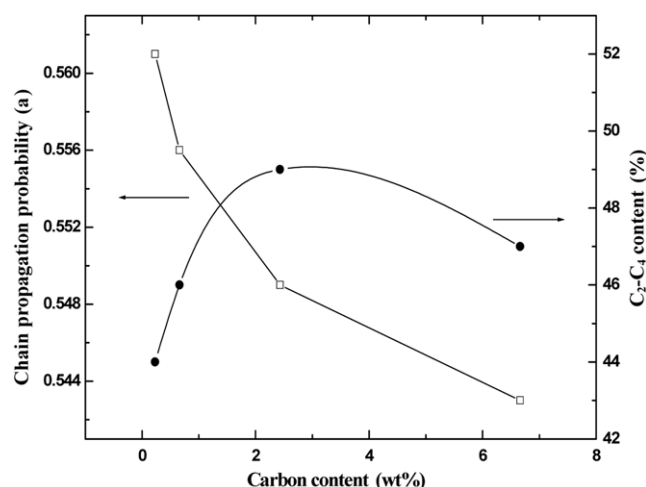
Fig. 4. The effect of carbon content on chain propagation ability. Reaction conditions: P=1.5 MPa, T=603 K, WHSV=1.05 Nl/g$_{cat}$·h, H$_2$/CO=2/1.
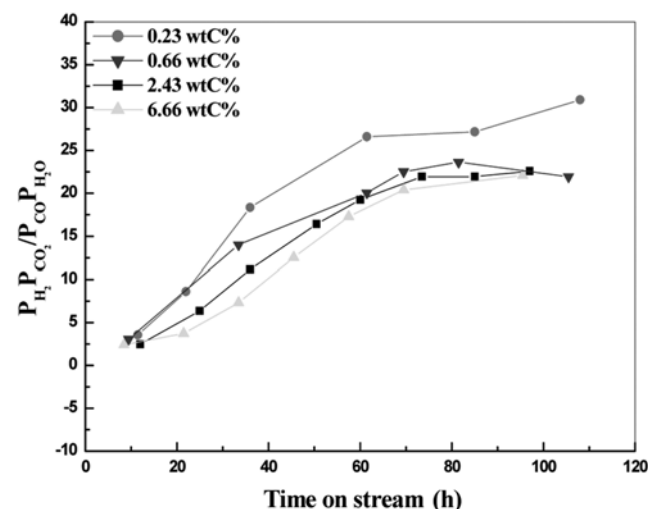
Fig. 5. The effect of carbon content on WGS reaction. Reaction conditions: P=1.5 MPa, T=603 K, WHSV=1.05 Nl/g$_{cat}$·h, H$_2$/CO=2/1.

tion of light hydrocarbons. The overall C_2-C_4 fraction of about 49 wt% (Table 3) was lower than the calculated value of 54%, which would be due to the secondary reactions such as hydrogenation and isomerization induced by the initial olefin readsorption [11]. In fact, the experimental value of C_2-C_4 fraction was always lower than that of the calculated.

8. Effect of Carbon Content on the WGS Reaction

Fig. 5 shows the effect of carbon content on the water gas shift (WGS) reaction. In our experiment, the value of $PCO_2PH_2/PCOPH_2O$ obtained under the same reaction conditions was used as an indication of the extent of the WGS reaction. Evidently, all the samples showed an increase of WGS reaction on the initial reaction period, which may have been caused by the partial oxidation of active component, since magnetite has been thought to favor the WGS reaction [16]. It was believed that the presence of carbon contacted with the active sites would provide a more hydrophobic surface [17], which could restrain the adsorption of water and then the WGS reaction would be inhibited. Furthermore, the inhibition of water gas shift (WGS) reaction may also reduce the hydrogenation ability of the catalyst, since the water gas shift (WGS) reaction could produce H_2 and may promote the adsorption of H_2 directly on the surface of the catalysts. So the presence of carbon inhibited the WGS reaction, which further restricted the direct adsorption of H_2 and reduced the hydrogenation ability. The unchanged CH_4 content with increasing carbon content confirmed the conclusion discussed above. Moreover, the presence of carbon would prevent the particles from sintering and stabilize the catalysts to prevent the carburization of iron, since the formation of iron carbide was thought to promote the formation of heavy hydrocarbons [18-20]. Therefore, it could be concluded that the formation of carbon not only promoted the interaction of iron and manganese as discussed above, but also reduced the hydrogenation of the catalyst and prevented the formation of heavy hydrocarbons. The slight decrease of olefin selectivity may be caused by the decrease of surface potassium content with increasing carbon content.

CONCLUSION

The role of carbon formed in situ by sol-gel method over Fe-Mn catalyst was investigated for CO hydrogenation. All the samples showed high activity and high selectivity to light olefins with O/P>4.5 in the catalytic test. With increasing carbon content, light hydrocarbon products were favored and the CH_4 selectivity was controlled. Also, the formation of carbon promoted the interaction of iron and manganese, and iron-manganese mixed crystallite was favored. Moreover, the formation of carbon provided a more hydrophobic surface, which inhibited the water gas shift reaction and reduced the hydrogenation ability of the catalysts.

ACKNOWLEDGMENT

REFERENCES

1. S. Ch. Roy, H. L. Prasad, P. Dutta, A. Bhattacharya, B. Singh and S. Kumara, *Appl. Catal. A: General*, **220**, 153 (2001).
2. K. Y. Park, W. K. Seo and J. S. Lee, *Catal. Letters*, **11**, 349 (1991).
3. K. J. Yoon and E. J. Kim, *Korean J. Chem. Eng.*, **12**, 221 (1995).
4. F. Tihay, A.C. Roger, A. Kiennemann and G. Pourroy, *Catal. Today*, **58**, 263 (2000).
5. J. K. Jeon, Ch. J. Kim, Y. K. Park and S. K. Ihm, *Korean J. Chem. Eng.*, **21**, 365 (2004).
6. J. Barrault and C. Renard, *Appl. Catal.*, **4**, 133 (1985).
7. Y. Yang, H. W. Xiang, Y. Y. Xu, L. Bai and Y. W. Li, *Appl. Catal. A: General*, **266**, 181 (2004).
8. X. G. Li, B. Zhong, S. Y. Peng and Q. Wang, *Catal. Letters*, **23**, 245 (1994).
9. L. Y. Xu and Q. X. Wang, *Catal. Letters*, **31**, 253 (1995).
10. J. Venter, M. Kaminsky, G. L. Geoffroy and M. A. Vannice, *J. Catal.*, **103**, 450 (1987).
11. R. A. Dictor and A. T. Bell, *J. Catal.*, **97**, 121 (1986).
12. X. G. Li, J. Y. Shen, B. Zhong, Y. Chen, S. Y. Peng and Q. Wang, *Hyperfine Interaction*, **69**, 867 (1991).
13. I. R. Leith and M. G. Howden, *Appl. Catal.*, **37**, 75 (1988).
14. M. Janardanarao, *Ind. Eng. Chem. Rev.*, **29**, 1735 (1990).
15. A. Machocki, *Appl. Catal.*, **70**, 237 (1991).
16. H. Arakawa and A. T. Bell, *Ind. Eng. Chem. Process Des. Dev.*, **22**, 97 (1983).
17. M. L. Cubeiro, H. Morales, M. R. Goldwasser, M. J. Pérez-Zurita, F. González-Jiménez and C. Urbina de N, *Appl. Catal. A: General*, **189**, 87 (1999).
18. G. B. Raupp and W. N. Delgass, *J. Catal.*, **58**, 361 (1979).
19. G. B. Raupp and W. N. Delgass, *J. Catal.*, **58**, 348 (1979).
20. D. B. Bukur, L. Nowicki, R. K. Manne and X. S. Lang, *J. Catal.*, **155**, 366 (1995).